communications physics

ARTICLE

https://doi.org/10.1038/s42005-022-01048-1 OPEN

Hidden magnetic texture in the pseudogap phase of high-Tc $YBa_2Cu_3O_{6.6}$

Dalila Bounoua [1✉], Yvan Sidis [1], Toshinao Loew[2], Frédéric Bourdarot [3], Martin Boehm [3], Paul Steffens [3], Lucile Mangin-Thro [3], Victor Balédent [4] & Philippe Bourges [1✉]

Despite decades of intense research, the enigmatic pseudo-gap (PG) phase of superconducting cuprates remains unsolved. In the last 15 years, various symmetry breaking states were discovered in the PG phase, including an intra-unit cell (IUC) magnetism, which preserves the lattice translational (LT) symmetry but breaks the time-reversal and parity symmetries, and an additional incipient charge density wave breaking the LT symmetry. However, none of these states can (alone) account for the partial gapping of the Fermi surface. Here we report a hidden LT-breaking magnetism using polarized neutron diffraction. Our measurements reveal magnetic correlations, in two different underdoped $YBa_2Cu_3O_{6.6}$ single crystals that set in at the PG onset temperature with (i) a planar propagation wave vector $(\pi, 0) \equiv (0, \pi)$, yielding a doubling or quadrupling of the magnetic unit cell and (ii) magnetic moments mainly pointing perpendicular to the CuO_2 layers. The LT-breaking magnetism is at short-range suggesting the formation of clusters of 5–6 unit cells. Together with the previously reported IUC magnetism, it yields a hidden magnetic texture of the CuO_2 unit cells hosting loop currents, forming large supercells that may be helpful for elucidating the PG puzzle.

[1] Université Paris-Saclay, CNRS-CEA, Laboratoire Léon Brillouin, 91191 Gif sur Yvette, France. [2] Max Planck Institute for Solid State, Heisenbergstrasse 1, research, 70569 Stuttgart, Germany. [3] Institut Laue-Langevin, 71 avenue des Martyrs, Grenoble 38000, France. [4] Université Paris-Saclay, Laboratoire de Physique des Solides, Orsay 91405 CEDEX, France. ✉email: dalila.bounoua@cea.fr; philippe.bourges@cea.fr

The phase diagram of high temperature cuprate superconductors is dominated by the mysterious PG phase overhanging the unconventional d-wave superconducting (SC) state[1–3]. A fundamental property of the PG is a partially gapped electronic spectrum whose origin has been under hot debate and deep experimental and theoretical scrutiny since its discovery[4]. A wide set of experimental results report the onset of broken discrete Ising (Z_2) symmetries at the same characteristic temperature T* where the electronic PG opens[5]. The discrete broken symmetries are: lattice rotation (C_4)[6–8], interpreted in terms of an (Ising) nematic order, inversion or parity as shown by second harmonic generation measurements[9] and time-reversal as reported by polarized neutron diffraction[10–16], circularly polarized angle resolved photo-emission spectroscopy[17] and muon spin spectroscopy[18]. The time-reversal and parity symmetry breakings are usually associated with a translationally invariant or Intra-Unit Cell magnetism ($\boldsymbol{q}=0$ or IUC-magnetism), either carried by loop currents (LC)[19–23] or by magnetic multipoles[24–26]. The detection of such objects is extremely challenging owing to the weakness of the corresponding signal, which is further partly hidden by the structural response during a scattering experiment[10–16]. However, to date, the reported IUC pattern preserves the LT symmetry. A large Fermi surface is thus conserved and none of the IUC related broken discrete symmetries can induce the needed electronic gap[1,27]. Meanwhile, the electron pockets observed at high magnetic field and low temperature in the PG phase[2,3] must originate from a phase breaking LT symmetry.

In the same region of the phase diagram, at lower temperature than T*, an incipient charge density wave (CDW) that competes with SC and breaks the LT and C_4 symmetries was extensively reported[1,2]. The short-range CDW induces a lattice superstructure leading to a uni/bi-axial response at incommensurate planar wave-vectors in reciprocal space $q_{CDW}=(0,\pm\epsilon)$ and/or $(\pm\epsilon,\ 0)$, with $\epsilon\sim0.3$ in reduced lattice units ($r.l.u$) in $YBa_2Cu_3O_{6+x}$ (YBCO). At zero magnetic field, CDW modulations are quasi-2D and weaken when entering the SC state at temperatures $T<T_c$. Upon applying either an external magnetic field along the c-axis[28] or a uni-axial pressure along the a-axis[29], 3D CDW correlations develop with a uni-axial character along the b-axis (direction of the underlying CuO chains in YBCO, see Fig. 1a). Although the incipient CDW breaks LT symmetry, its onset temperature T_{CDW} remains well below T^*, deep into the PG phase, and can thus not be alone at the origin of the opening of the electronic gap. This conclusion is further reinforced by recent Hall transport measurements[30].

To describe this manifold problem and reconcile the seemingly unrelated discrete symmetry breakings and occurrence of the electronic gap, new theoretical approaches invoking the concept of intertwined states were elaborated[1]. Apart from the IUC magnetism arising from LC order, other unconventional magnetic correlations involving alternative LT-symmetry breaking charge current patterns have been discussed in cuprates. For instance, starting from a collinear homogeneous antiferromagnetic (AF) Mott insulator (zero hole-doping, localized $S=\frac{1}{2}$ spins on Cu atoms) with a magnetic response at the planar wave-vector $\mathbf{q}_{AF}=(0.5,0.5)$, hole-doping was proposed to destabilize the AF state towards a spin-liquid state characterized by a staggered flux phase (π-flux)[31], also described as a d-wave charge density wave (DDW) state[32]. This state exhibits staggered LC, yielding an orbital magnetic response at $\mathbf{q}_{DDW}=\mathbf{q}_{AF}$. Note, however, that the Cu-spin moments are locked within the CuO_2 layers (planar anisotropy)[33], whereas the LC orbital moments are expected to be perpendicular to the CuO_2 layers. Despite several attempts, neutron diffraction measurements failed to prove the existence of such a phase[14,34].

Here, using polarized neutron diffraction, we report magnetic correlations at commensurate planar $\mathbf{q}$-wave-vectors $(q,0)\equiv(0,q)$ with $\boldsymbol{q}=1/2$ that correspond to a lattice symmetry breaking and appear to be tightly bound to the PG physics in the underdoped $YBa_2Cu_3O_{6.6}$ material. This magnetim is at short-range suggesting the formation of clusters of 5-6 unit cells that can be associated with a hidden magnetic texture emerging out the CuO_2 unit cells hosting loop currents.

Results

We performed elastic polarized neutron diffraction (PND) experiments on three Triple Axis Spectrometers (TAS): 4F1 at Orphée reactor-Saclay, IN22 and Thales at Institut Laue-Langevin-Grenoble, operating at different wavelengths and using different neutron polarization setups (see Methods). The TAS were equipped with longitudinal XYZ polarization analysis (XYZ-PA, see Methods), a powerful technique to selectively probe and disentangle the magnetic response from the nuclear one with no assumptions on the background. The samples were studied either in (1,0,0)/(0,0,1) or (1,0,0)/(0,1,0) scattering planes such as wave-vectors of the form $(H,0,L)$ or $(H,K,0)$ in momentum space were accessible. In the following, the wave-vectors are indexed in reduced lattice units (r.l.u.) of $(\frac{2\pi}{a},\frac{2\pi}{b},\frac{2\pi}{c})$ where a, b and c stand for the lattice parameters of the sample (See Methods and Supplementary Note 1 for details). We carried out our investigations in two different $YBa_2Cu_3O_{6+x}$ samples: a twinned YBCO-t sample and a detwinned sample YBCO-d[10,15], with close compositions (nominal $x=0.6$) and with similar hole-doping ($p\sim0.11$) and critical temperatures ($T_c=61$ and 63 K) but with different oxygen ordering the CuO chains.

Momentum dependence. Using XYZ-PA, we uncovered a magnetic peak centered at $\mathbf{Q}=(0.5,0,0.5)$ in YBCO-t, as shown by the H-scan along (H,0,0.5) (Fig. 1b). The magnetic signal can be described by a Gaussian profile, broader than the instrumental resolution. After deconvolution, its intrinsic linewidth—half width at half maximum (HWHM)—is $\Delta_H=0.03\pm0.01$ r.l.u. This corresponds to a finite correlation length along the a-axis of $\xi_a=\frac{a}{2\pi\Delta}\simeq 20\pm6$Å, corresponding to ~5 planar unit-cells. A rocking scan across (0.5,0,0.5) allowed us to confirm the intrinsic origin of the magnetic signal, excluding extrinsic scattering due to powder lines from a parasitic magnetic phase (see Supplementary Note 2 and Supplementary Fig. 1).

The L-scan of Fig. 1c was performed in the non-spin-flip NSF_X channel and shows a nuclear scattering at $\mathbf{Q}$-positions of the form $(0.5,0,L)$ with L integer. This peculiar structure factor is due to the characteristic Ortho-II structure of the CuO chains, running parallel to the b-axis as represented in Fig. 1a[35]. The same scan along the $(0.5,0,L)$ direction, obtained using XYZ-PA, shows a broad magnetic scattering, at odds with the Ortho-II oxygen ordering in the CuO chains (Fig. 1d). This rules out the chains as the host of the new-found magnetic signal rather pointing to the CuO_2 planes (Fig. 1a) as the origin of the magnetic response, breaking the LT invariance ($\boldsymbol{q}=1/2$). The diffuse magnetic signal along the $(0.5,0,L)$ trajectory of Fig. 1d further underlines the absence of magnetic correlations along the c-axis. For both scans along H and L, raw data for YBCO-t are shown in Supplementary Fig. 2.

To ascertain the existence of the $\boldsymbol{q}=1/2$ magnetism and unravel scattering from CuO chains and CuO_2 planes, we carried out further PND investigations in the detwinned sample, YBCO-d. Fig. 2 shows the PND results along several directions in momentum space defined in Fig. 2f. (Raw data scans for YBCO-d are shown in Supplementary Figs. 3 and 4). Figure 2a depicts a scan along the H direction in the spin-flip SF_X channel revealing

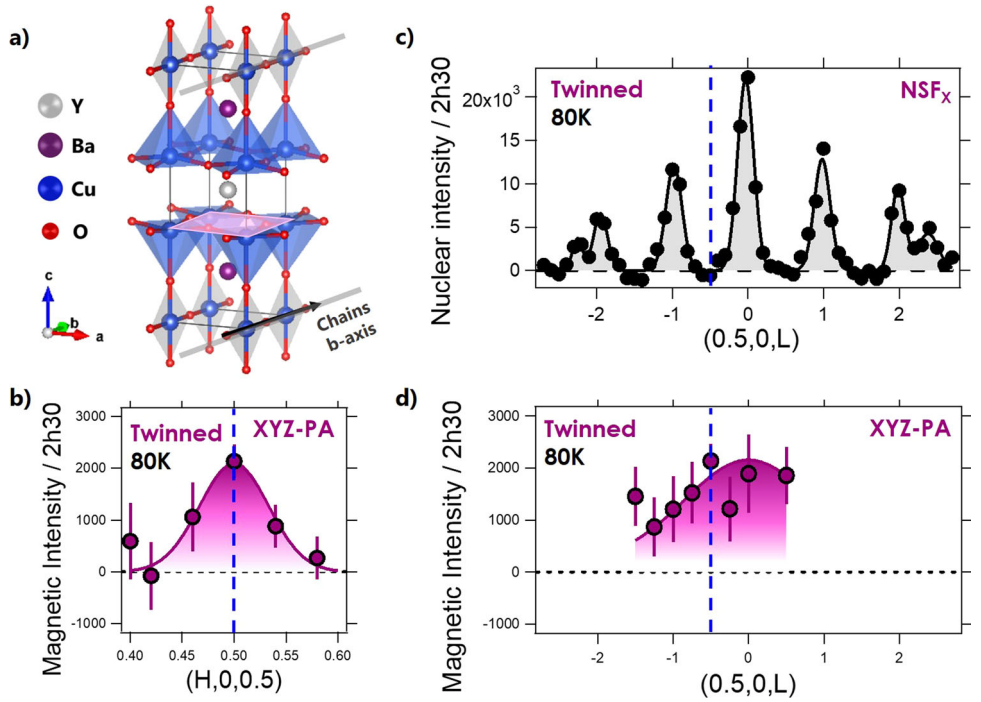

Fig. 1 Commensurate magnetism in twinned $YBa_2Cu_3O_{6.6}$ (YBCO-t). **a** Crystal structure of $YBa_2Cu_3O_{6+x}$ with the CuO chains running along the b-axis (gray shaded arrow) and the CuO_2 planes represented by the pink shading. **b** Scan in momentum space along the H direction across (0.5,0,0.5) showing the magnetic scattering extracted from XYZ polarization analysis (XYZ-PA). The magnetic scattering is fitted by a Gaussian line centered at (0.5,0,0.5). **c** Background subtracted scan in momentum space along the (0.5,0,L) direction in the non-spin-flip (NSF$_X$) channel. The peaks in the NSF$_X$ channel correspond to nuclear scattering from the Ortho-II oxygen chains superstructure. **d** Q-dependence of the magnetic intensity along the (0.5,0,L) trajectory as extracted from full XYZ-PA in YBCO-t. Data in **b**–**d** were measured on 4F1 at 80K with the sample aligned in the (1,0,0)/(0,0,1) scattering plane. Lines are fits by a sum of Gaussian peaks to the data. Error bars represent one standard deviation. Raw data are given in Supplementary Fig. 2.

the occurrence of a magnetic peak, centered at $(0.5,0,0) \equiv (\pi, 0)$. As in YBCO-t, the signal is at short-range with $\Delta_H = 0.025 \pm 0.01$ r.l.u. given by the fit with a Gaussian profile. This corresponds to $\xi_a = \frac{a}{2\pi\Delta} \simeq 24 \pm 4$Å, which represents correlations over ~ 6 unit cells, consistent with the value deduced in the YBCO-t sample. The same scan in the NSF$_X$ channel Fig. 2b reveals two nuclear peaks at $H = 0.385$ and 0.625, inherent to the Ortho-VIII oxygen ordering of the CuO chains[35] in that YBCO-d sample[36], which leads to nuclear satellites at $\mathbf{q}_{Ch} = (H \pm 0.125, 0, 0)$ where no magnetic signal occurs (Fig. 2a). The absence of magnetic scattering at the characteristic $\mathbf{q}_{Ch}$ positions confirms the CuO_2 planes as the origin of the magnetic response at $H = 0.5$.

We further performed a survey of the momentum dependence of the magnetic signal in the detwinned YBCO-d sample, where a and b directions are clearly identified, to determine its planar structure factor. Figure 2c shows the resulting magnetic intensity along the $(H, 0.5, 0)$ trajectory, as given by XYZ-PA. The H-scan reveals as well a magnetic peak centered at $(0, 0.5, 0) \equiv (0, \pi)$ while no magnetic intensity is seen at $\mathbf{q}_{AF/DDW} = (0.5, 0.5, 0) \equiv (\pi, \pi)$. The observed magnetic pattern is then found along both CuO-bond directions with actually a very similar intensity. This indicates a short-range either uni-axial (with domains) or bi-axial magnetism leading to a local doubling or quadrupling (2×2) of the unit cell, never reported previously. Additional measurements with the sample aligned within $[a, c]$ plane allowed us to elucidate the L-dependence of the out-of-plane magnetic correlations. Figure 2d shows an L-scan across $(0.5, 0, 0)$ in the SF$_X$ channel highlighting a broad magnetic peak, centered at $(0.5, 0, 0)$. The extracted correlation length (from a fit by a Gaussian function) $\xi_c \simeq 13 \pm 1$ Å is very short and does not exceed the size of ~ 1 unit-cell in the c direction ($\Delta_L = 0.14 \pm 0.01$ r.l.u. HWHM after deconvolution).

We further investigated the structure factor of the (2×2) magnetism through XYZ-PA measurements at additional equivalent **Q**-points in other Brillouin zones. The results are reported in Fig. 2e and show the occurence of magnetic intensity at wavevectors of the form (0.5,1,0) as well, whereas the limited statistics at (1.5,0,0) prevents from drawing a clear conclusion about the existence of a magnetic response and requires further investigations.

Temperature dependence. To determine the onset temperature of the short-range $\boldsymbol{q} = 1/2$ magnetism, we measured the temperature dependence of the signal at $(0.5, 0, 0)$ in YBCO-d, both in the SF$_X$ channel and using XYZ-PA. Figure 3a shows the total scattered magnetic intensity that splits into a leading out-of-plane magnetic component $\mathbf{I}_c$ displaying an order parameter-like temperature dependence in Fig. 3b and a subsidiary in-plane magnetic component, $\mathbf{I}_b$, which at variance, remains almost constant as a function of temperature Fig. 3c. Our measurements show that the onset temperature for the dominating $\mathbf{I}_c$ magnetic component is $T^* \sim 235$ K. The temperature dependence of the magnetic signal at $(0, 0.5, 0)$ as deduced from $XYZ - PA$ analysis reproduces the same Ising-like orientation of the magnetic moment, with a similar amplitude as at $(0.5, 0, 0)$: a major $\mathbf{I}_c$, out-of-plane component, arises at $T^* \sim 235$K following the same order parameter-like temperature dependence (Supplementary Fig. 5). The H-scans across $(0.5, 0, 0)$ on Fig. 3d, e show the drop of the magnetic signal from 10 to 300 K, respectively. The data correspond to measurements in the SF$_{X,Y,Z}$ channels. Note in Fig. 3d that the magnetic signal in the **X** channel corresponds to six times the statistical noise related to the background. However, using

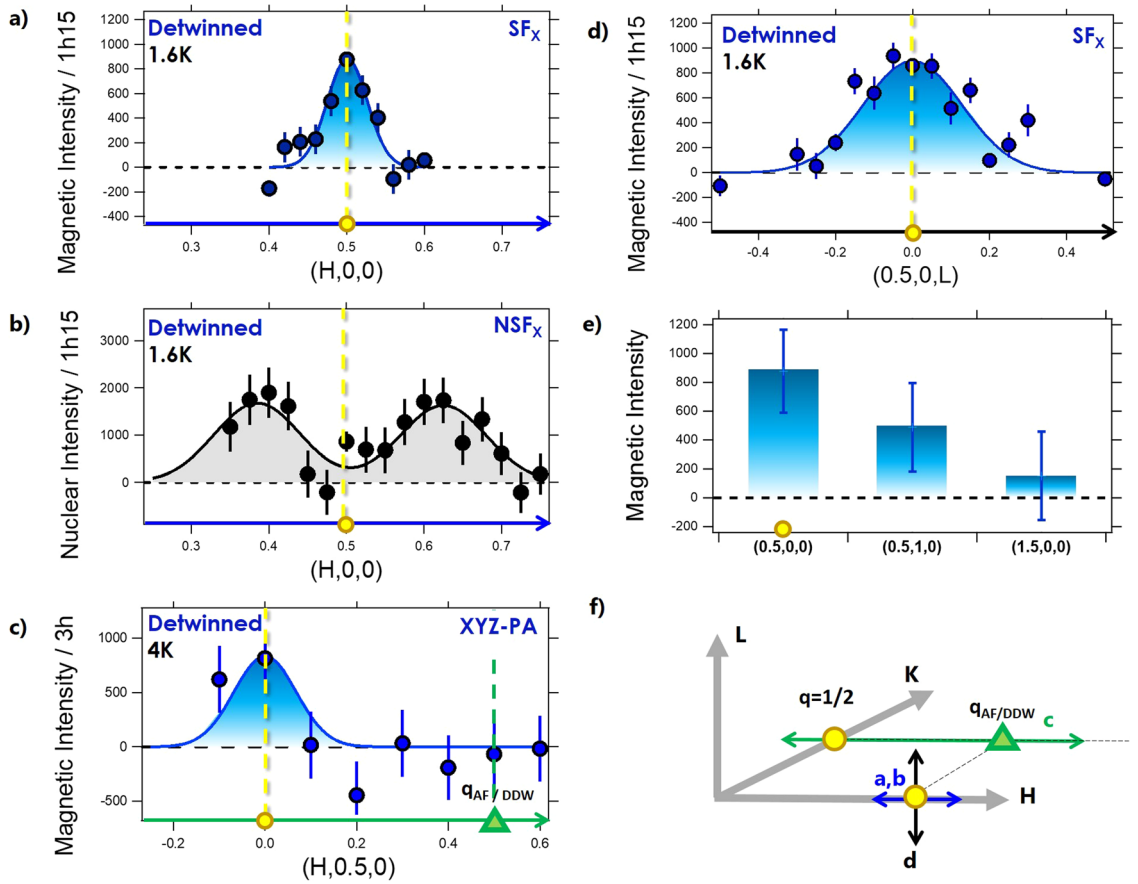

Fig. 2 Biaxial planar short-range magnetism in twin-free $YBa_2Cu_3O_{6.6}$ (YBCO-d). **a** Background subtracted scan along (H,0,0) in the spin-flip (SF_X) channel. The magnetic intensity appears as a Gaussian signal centered at (0.5,0,0). **b** Background subtracted scan along (H,0,0) in the non-spin-flip (NSF_X) channel showing the nuclear scattering from the (Ortho-VIII) type chains superstructure. **c** Scan along $\mathbf{Q} = (H,0.5,0)$ obtained through XYZ polarization analysis (XYZ-PA) showing a magnetic signal centered at $H = 0$. **d** Background subtracted scan along $\mathbf{Q} = (0.5,0,L)$ in the spin-flip (SF_X) channel. The magnetic intensity appears as a Gaussian signal centered at (0.5,0,0). **e** Magnetic intensity resulting from XYZ-PA at different wave-vectors in the reciprocal space: (0.5,0,0), (0.5,1,0) and (1.5,0,0). **f** 3D representation of the reciprocal space showing the momentum scans performed in **a**–**d**. Data in **a**, **b**, **d**, **e** were measured on IN22 at 1.6K with the sample aligned in the (1,0,0)/(0,0,1) scattering plane. Data in **c** were measured on 4F1 at 4K with the sample aligned in the (1,0,0)/(0,1,0) scattering plane. Lines are fits by a sum of Gaussian peaks to the data. Error bars represent one standard deviation. Raw data are given in Supplementary Fig. 3.

unpolarized neutron diffraction, the magnetic scan would remain totally hidden by the large and modulated nuclear scattering from the chains.

Further, the temperature dependence of the out-of-plane magnetic response, $\mathbf{I}_c$, matches the one reported for the IUC-magnetism (Supplementary Fig. 5): $\mathbf{I}_c$ sets-in at $T \simeq T^*$, the PG onset temperature as reported from resistivity measurements[37], and of $T \sim T_{mag}$, the onset temperature for the $\boldsymbol{q} = 0$ magnetic order[10,14], suggesting a common origin of both the IUC magnetic order and the short-range $\boldsymbol{q} = 1/2$ magnetism reported here. On general grounds, because it breaks LT, the $\boldsymbol{q} = 1/2$ magnetism could be an alternative candidate for the opening of the PG state, potentially solving a long-standing question. Along the same line of thought, it could as well play a significant role in the electron pockets formation[2] yielding a Fermi surface reconstruction known to be exclusively occurring within the PG state.

Discussion

Our comprehensive set of PND data gives a coherent picture for the $\boldsymbol{q} = 1/2$ magnetism occuring at commensurate $(\pi, 0) \equiv (0, \pi)$ in high-T_c superconducting $YBa_2Cu_3O_{6.6}$. First, the location of the observed magnetism is clearly distinct from $\mathbf{q}_{AF} \equiv (\pi, \pi)$. This rules out various reported magnetic patterns, namely the antiferromagnetic spin order, π-flux or DDW phases[31,32], all phases located at the commensurate (π, π) position, or the Spin Density Wave (SDW) located at incommensurate position $\mathbf{q}_{SDW} = \mathbf{q}_{AF} \pm (\delta, 0)$ or $(0, \delta)$ with $\delta \sim 0.1$ revealed by spin fluctuations induced by zinc impurity[38]. Second, the occurence of both propagation vectors $\mathbf{q}_1 = (0.5, 0, 0)$ and $\mathbf{q}_2 = (0, 0.5, 0)$ suggests a biaxial ordering with a double-$\mathbf{q}$ antiferromagnetic structure, corresponding to a quadrupling (2×2) of the unit cell. However, a uniaxial ordering, doubling the unit cell along each direction of the CuO bonds, can as well account for the observed patterns, assuming equi-populated magnetic domains along each direction. This can happen even in the detwinned sample if the magnetic domains do not depend on the underlying orthorhombic structure.

We considered several models that can reproduce the scattering selection rules for the $\boldsymbol{q} = 1/2$ magnetism. Fig. 4 shows three different magnetic patterns corresponding to 2×2 larger unit cells and involving either spin or orbital magnetic moments at one Cu-site over 2 (Fig. 4a) with an antiferromagnetic coupling along the unit cell diagonal, a loop currents model (Fig. 4b) corresponding to the smallest possible domain with a period of $2Pa$ ($P = 1$, a is the lattice parameter) of LC supercell recently

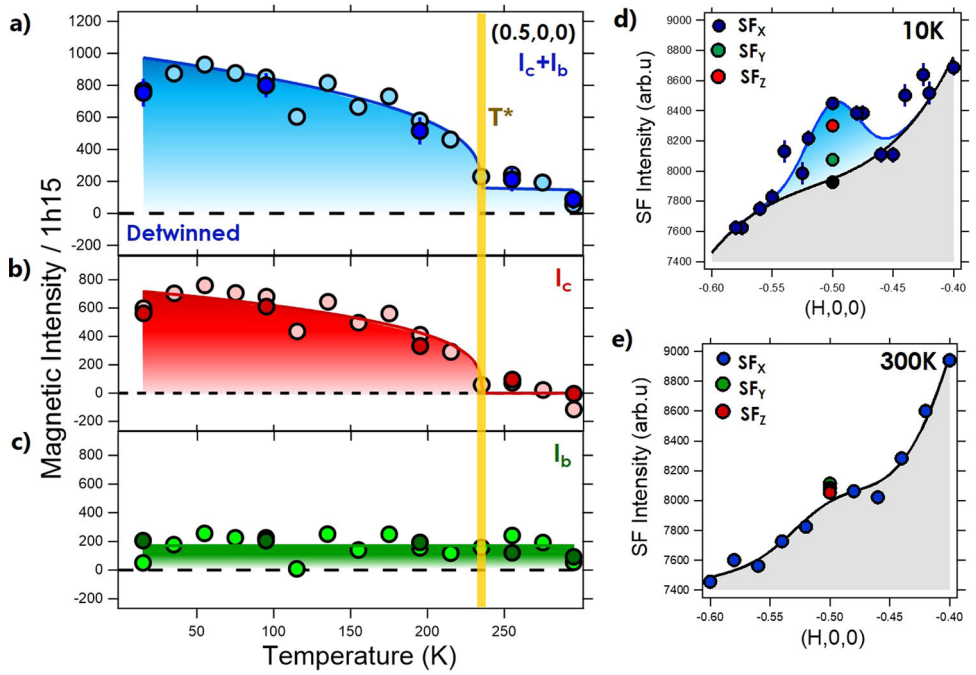

Fig. 3 Temperature dependence of the biaxial magnetism in detwinned $YBa_2Cu_3O_{6.6}$ (YBCO-d). a Temperature dependence of the magnetic intensity measured at (0.5,0,0) as extracted from XYZ polarization analysis (XYZ-PA) (dark blue circles) and background subtracted SF_X data (light blue circles). Temperature dependence of **b** the out-of-plane magnetic response, $\mathbf{I}_c$, (dark red circles) and **c** the in-plane magnetic scattering, $\mathbf{I}_b$, (dark green circles) as extracted from XYZ-PA. Light red circles in **b** correspond to $\mathbf{I}_c$ as extracted from the SF_X data in **a** subtracted from the fit to the in-plane component in **c**. Light green circles in **c** correspond to $\mathbf{I}_b$ as extracted from the SF_X data in **a** subtracted from the fit to the out-of-plane component in **b**. The blue symbols in panel **a** correspond to the sum $\mathbf{I}_c + \mathbf{I}_b$. H-scans across (0.5,0,0) measured in the Spin Flip ($SF_{X,Y,Z}$) channels at **d** 10K and **e** 300 K. The magnetic intensity appears as a Gaussian signal centered at 10K and drops at 300K in YBCO-d. Data in **a**–**e** were measured on Thales with the sample aligned in the (1,0,0)/(0,0,1) scattering plane. Error bars (sometimes smaller than the points size) represent one standard deviation. Raw data of **a**, **b** are given in Supplementary Fig. 5.

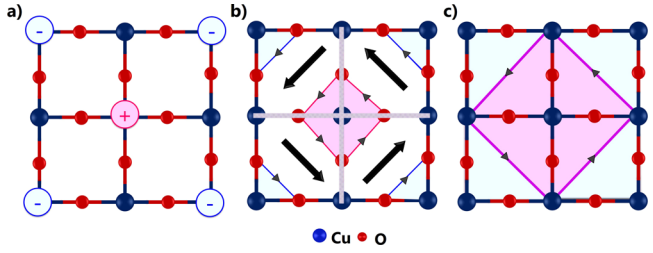

Fig. 4 Possible models for the biaxial (2a x 2a where a is the cell parameter) planar magnetism in $YBa_2Cu_3O_{6.6}$. a Magnetic moments at one over two Cu-site. **b** Loop currents pattern turning clockwise (in blue) and anti-clockwise (in pink), corresponding to the pattern label $P = 1$ in ref. [27]. Each cell (size a x a) carries an anapole moment (black arrow). The pattern comprises 4 loop currents states where the anapole undergoes a 90° rotation between adjacent cells. **c** Loop currents pattern with $a\sqrt{2}$x$a\sqrt{2}$ loop size, consisting in a 45° rotation of the *d*-wave charge density wave (DDW) pattern with currents running between Cu-sites. All models in **a**–**c** reproduce the experimentally measured structure factor (Supplementary Note 2).

proposed to break the lattice translation symmetry[27] and where the anapole undergoes a 90° rotation at each adjacent unit cell[5], or a staggered loop currents phase with currents running along the diagonals of the CuO_2 planes (Fig. 4c). All these patterns nicely agree with the measured structure factor (Supplementary Note 3). However, the magnetic moment predominantly observed perpendicular to the CuO_2 layers does not support an interpretation in terms of *Cu* spins that are locked within the CuO_2 planes owing to their strong XY spin anisotropy[33]. It instead favors loop current patterns as the ones shown in Fig. 4b, c where, in principle, orbital moments should be perpendicular to the planes where currents are confined[19].

Following all these observations, one can build real space pictures based on loop currents to account for both the IUC magnetism and the hidden $\boldsymbol{q} = 1/2$ magnetism. As originally proposed in ref. [39,40], LCs are conveniently characterized by four degenerate states that can be represented by anapole moments pointing along the four planar unit cell diagonals as displayed in Fig. 5a where each color corresponds to a given anapole orientation. Using these four basic states, one can build an anapole-vortex-like phase represented in Fig. 5b that also describes the $\boldsymbol{q} = 1/2$ magnetism. It is similar to Fig. 4b but now with anapoles located on the Cu-sites[27]. The pattern is both chiral and parity-breaking, and therefore of *mm*2 symmetry as it has been recently reported from photogalvanic experiments[41]. The amplitude of the total magnetic scattering has been estimated in absolute units after calibration by the intensity of the reference (1,0,0) nuclear Bragg peak. This magnetic intensity is weak and represents only ~0.3 ± 0.1 mbarn once integrated in momentum space, which is about 10-15 times lower than the one reported for the long-range ordered ($\boldsymbol{q} = 0$) IUC-magnetism at the (1,0,0) position[10,12,14,15]. This explains why the magnetic signal remained hidden in previous experiments.

A natural question is then what can be the interplay between both LC phases with distinct propagation wave-vectors, $\boldsymbol{q} = 0$ and $\boldsymbol{q} = 1/2$? First, the short-range nature of the observed correlations implies 2×2 LC islands of only about ~20–25 Å. This therefore precludes a homogeneous distribution of magnetic moments with 2×2 correlations superimposed on IUC magnetism that respect LT. Inhomogeneous pictures in real space should

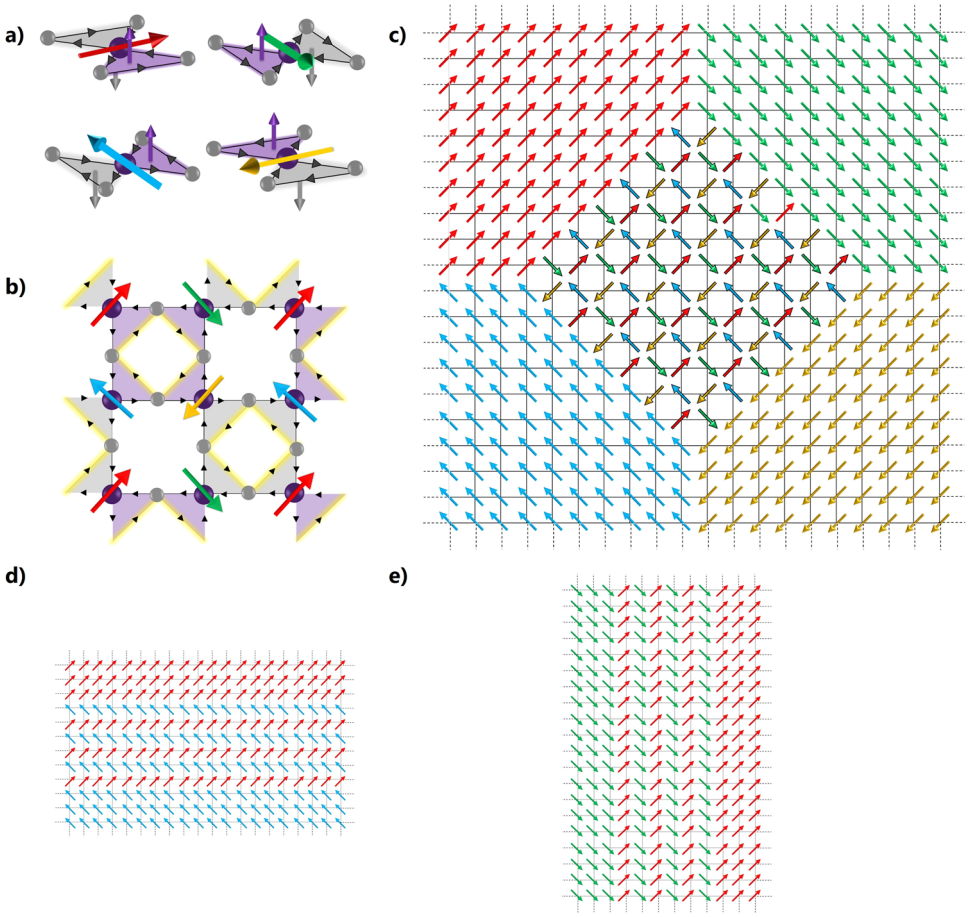

Fig. 5 Hidden magnetic texture from the modelization of $q = 1/2$ short-range and intra-unit cell (IUC) magnetism observed by polarized neutron diffraction. a Four possible degenerate ground states of loop currents (LC)[19,39,40]. The gray and purple arrows represent magnetic moments along the **c** axis whereas the four other arrows represent anapoles centered at the Cu-site of each of the four states. **b** 2 × 2 loop currents pattern that can account for the $q = 1/2$ magnetism. The currents circulate clockwise (in gray) and anti-clockwise (in purple). The four states are represented by anapoles undergoing a 90° rotation between adjacent domains. **c** Example of a 2D magnetic texture with 20 × 20 unit cells paved by anapoles (LC states). The central cluster with 2 × 2 LC patterns describe the $q = 1/2$ short-range magnetism whereas the IUC magnetic signal arises from the larger color domains. **d**, **e** Similar LC construction for horizontal and vertical 1D domains. In panels **c**–**e**, only the anapoles are represented having the four possible orientations.

be considered instead, revealing a hidden anapolar or magnetic texture. How can a unifom LC order coexist with a modulated one at short-range? This can be accounted for by locating the short-range modulated phase at the domains walls between the long-range uniform ($q = 0$) domains. Along the same line of thought and by analogy with the electronic liquid crystals where smectic modulations coexist with an IUC nematicity[42], one can speculate about the coexistence of a "smectic" short range ($q = 1/2$) 2 × 2 LC magnetism with a "nematic" ($q = 0$) longer range magnetism (ferro-anapolar).

Let us first remind that the neutron intensity (I) is proportional to the number of magnetic sites (N) times the square of the magnetic moment, m: $I \propto Nm^2$. To give the order of magnitude, a magnetic intensity of ~ 0.3 mbarn would correspond to an estimate of the magnetic moment per loop current triangle of $m_{tr} \sim 0.025\ \mu_B$ (see supplementary note 3) under the assumption that the pattern of Fig. 5b has a homogeneous distribution of moments (i.e. where all unit cells contribute to the magnetic signal). However, as this assumption is not consistent with the data (short-range magnetism), it yields instead a picture of finite clusters with larger magnetic moments. According to the inhomogeneous picture of coexisting orders, the observed amplitudes of the $q = 1/2$ magnetism (located at the boundaries separating larger $q = 0$ domains) would determine the volume fraction of both magnetic patterns within the crystal. In contrast to the homogeneous picture, the 10–15 times weaker intensity of the $q = 1/2$ magnetism instead implies that 10–15 less sites belongs to the 2 × 2 LC clusters assuming the same magnetic moment in each unit cell as the one extracted from the IUC magnetism[10,12,14].

Real space pictures can be built following these requirements. As an example, Fig. 5c shows a pattern of anapoles over 20 × 20 unit cells that represents such a topological arrangement of anapoles (and consequently related loop currents and orbital magnetic moments). Its calculated structure factor matches the observations of the short-range magnetism at both (0.5,0,0) and (0,0.5,0) and longer range IUC magnetism. This picture can be extended to a larger number of unit cells (for instance with more than one 2 × 2 LC cluster) with only two requirements: (i) the clusters should be isolated and (ii) should represent in total about a tenth of the unit cells. The longer range uniform LC domains form the large supercells (of $2P \times 2P$ size) introduced by C.M. Varma[27] to account for the Fermi arcs in the PG state. Note however that the $P = 1$ clusters reported here cannot explain the observed Fermi arcs or magneto-oscillations in this model. LC supercells are predominantly characterized in momentum space by a set of satellites magnetic peaks located at $\pm \frac{1}{2P}$ from the atomic Bragg peak positions. As far as $P \gtrsim 10$, they would be

indistinguishable from a single peak at $\boldsymbol{q} = 0$ due to the limited momentum instrumental resolution of elastic PND experiments[5]. However, more experiments are necessary to clarify this point. Meanwhile, as far as the site occupation rule holds, 1D arrangements of anapoles either horizontal or vertical as shown in Fig. 5d, e could as well describe the data, with however an additional constraint of equi-populated domains along both directions. Note that the magnetic texture, through the domains size P, can vary noticeably within the crystal leading to a distribution of satellite peaks near the Bragg peaks with similar short-range $\boldsymbol{q} = 1/2$ magnetism. One can therefore envisage a vast range of possible hidden magnetic textures opened by the observation of short-range $\boldsymbol{q} = 1/2$ magnetism.

About the interplay of $\boldsymbol{q} = 0$ and $\boldsymbol{q} = 1/2$ magnetism, two interesting points should be emphasized. First, the data for the $\boldsymbol{q} = 1/2$ magnetism shows a larger moment pointing along the c-axis whereas the moments of $\mathbf{q} = 0$ are tilted with respect to the c-axis[14,43]. It should be stressed that both observations can be consistent as the planar contribution of the magnetic structure factor for both signals depends largely on the specific modeling of the planar component whose origin is still under discussion[5]. Next, the $\boldsymbol{q} = 0$ magnetism shows a planar anisotropy of the neutron intensity along both in-plane directions, suggesting a specific arrangement of anapoles within the bilayer[15]. Instead, the short-range $\boldsymbol{q} = 1/2$ domains show an isotropic signal. Here again, the LC correlations within the bilayer can be different for both signals because the 2×2 LC patterns are mixing the four anapolar directions. Clearly, more experimental data are necessary to settle these questions.

Finally, it is worth recalling that magnetic-sensitive local probes experiments (Nuclear Magnetic Resonance and Muon Spin Rotation) do not observe the expected static local magnetic fields of the magnetism reported by elastic PND measurements[5,44]. Instead, a fluctuating magnetic response in the PG state has been reported by Muon spectroscopy[18]. This suggests a magnetic texture slowly fluctuating at a ~10 ns time scale, encompassing the $\boldsymbol{q} = 0$ IUC magnetic response and the short-range $\boldsymbol{q} = 1/2$ magnetism. Both appear static in PND owing to the instrumental energy resolution of ~0.1 meV. The $\boldsymbol{q} = 1/2$ magnetic response and the previously reported $\boldsymbol{q} = 0$ signal together are related to a magnetic structure factor of a complex hidden magnetic texture (with large supercells of length scale $2P$ and a magnetic moment of ~0.1 μ_B in each unit cell). We hope the present work would motivate further experimental investigations in other cuprate families and other hole-doping levels as well as theoretical investigations to understand the role of the hidden magnetic texture in the phase diagram of high-T_c superconducting cuprates.

Methods

Samples. The polarized neutron diffraction study was performed on two different samples of same nominal composition $YBa_2Cu_3O_{6.6}$ although they exhibit different oxygen ordering within the CuO chains. The twinned sample (YBCO-t) ($T_c = 61$ K and hole-doping $p = 0.107$) is the same as the one used in ref. [10] with an Ortho-II oxygen ordering. It has a mass of ≈ 10 g and a mosaic spread of 1.5°, determined by performing rocking curves about the nuclear Bragg peaks. The twin-free sample (YBCO-d) has been obtained by methods described in ref. [36] ($T_c = 63$ K and hole-doping $p = 0.115$). It consists of co-mounted single crystal plates of about (20×20 mm^2) and exhibits an Ortho-VIII oxygen ordering. The total sample mass is ~2g and the measured mosaic spread is 2°. We used pseudo-tetragonal notations for the twinned sample, with $a = b = 3.85$ Å and $c = 11.75$ Å. The lattice parameters of the twin-free sample are $a = 3.82$ Å, $b = 3.87$ Å and $c = 11.75$ Å.

Polarized neutron diffraction (PND). The polarized neutron diffraction experiments were carried out on on three distinct triple axis spectrometers (TAS): 4F1, IN22 and Thales: the TAS 4F1 (Orphée reactor, Saclay) and the IN22 and Thales TAS (Institut Laue Langevin, Grenoble), which are described in more details in the Supplementary Note 1. These instruments are equipped with distinct neutron polarization set-ups and were operating with three distinct neutron wavelengths, to guarantee the reproducibility of the measurements. We used incident neutron wave-vectors of $\boldsymbol{k}_i = 2.57$ Å^{-1} on 4F1, $\boldsymbol{k}_i = 2.662$ Å^{-1} on IN22, and $\boldsymbol{k}_i = 1.5$ Å^{-1} on Thales. As detailed in the figure captions, the samples were either aligned in the (1,0,0)/(0,0,1) or (1,0,0)/(0,1,0) scattering planes, so that wave-vectors $\mathbf{Q}$ of the form $(H, 0, L)$ or $(H, K, 0)$ were accessible, respectively. H, K or L-scans were performed across positions of the form (0.5,0,0) or (0,0.5,0) in r.l.u. Both spin-flip (SF) and non-spin-flip (NSF) scans were done in order to crosscheck the absence of nuclear scattering at magnetic positions. Longitudinal XYZ- polarization analysis (XYZ-PA) was performed where, according to conventional notations, **X** stands for the direction of the neutron polarization parallel to **Q**, **Y** and **Z** polarization directions are both perpendicular to **Q**. **Y** is the in-plane orthogonal direction and **Z** is perpendicular to the scattering plane. On the different neutron instruments, we were using different devices to perform XYZ-PA as:

- MuPAD spherical polarization analysis device with zero magnetic field at the sample chamber on 4F1, for the twin-free $YBa_2Cu_3O_{6.6}$ sample. The incoming and outgoing beam polarizations are realized using Bender supermirrors.
- CRYOPAD spherical polarization analysis device with zero magnetic field at the sample chamber on IN22 and Thales for the twin-free $YBa_2Cu_3O_{6.6}$ sample. The incoming and outgoing beam polarizations are realized using Heusler crystals.

Data availability

The data obtained on IN22 at ILL are available at https://doi.org/10.5291/ILL-DATA.CRG-2776. The data obtained on Thales at ILL are available at https://doi.org/10.5291/ILL-DATA.4-02-600. The rest of the data that support the findings of this study is available from the corresponding authors upon request.

Received: 17 May 2022; Accepted: 19 October 2022;
Published online: 02 November 2022

References

1. Keimer, B., Kivelson, S. A., Norman, M. R., Uchida, S. & Zaanen, J. From quantum matter to high-temperature superconductivity in copper oxides. *Nature* **518**, 179–186 (2015).
2. Proust, C. & Taillefer, L. The remarkable underlying ground states of cuprate superconductors. *Annu. Rev. Condens. Matter Phys.* **10**, 409–429 (2019).
3. Varma, C. M. Colloquium: Linear in temperature resistivity and associated mysteries including high temperature superconductivity. *Rev. Mod. Phys.* **92**, 031001 (2020).
4. Alloul, H., Ohno, T. & Mendels, P. Y^{89} NMR evidence for a fermi-liquid behavior in $YBa_2Cu_3O_{6+x}$. *Phys. Rev. Lett.* **63**, 1700 (1989).
5. Bourges, P., Bounoua, D. & Sidis, Y. Loop currents in quantum matter. *Comptes Rendus Phys.* **22**, 7–31 (2021).
6. Sato, Y. et al. Thermodynamic evidence for a nematic phase transition at the onset of the pseudogap in $YBa_2Cu_3O_y$. *Nat. Phys.* **13**, 1074 (2017).
7. Lawler, M. et al. Intra-unit-cell electronic nematicity of the high-Tc copper-oxide pseudogap states. *Nature* **466**, 347–351 (2010).
8. Daou, R. et al. Broken rotational symmetry in the pseudogap phase of a high-Tc superconductor. *Nature* **463**, 519–522 (2010).
9. Zhao, L. et al. A global inversion-symmetry-broken phase inside the pseudogap region of $YBa_2Cu_3O_y$. *Nat. Phys.* **13**, 250–254 (2017).
10. Fauqué, B. et al. Magnetic order in the pseudogap phase of high-T_c superconductors. *Phys. Rev. Lett.* **96**, 197001 (2006).
11. Li, Y. et al. Unusual magnetic order in the pseudogap region of the superconductor $HgBa_2CuO_{4+\delta}$. *Nature* **455**, 372–375 (2008).
12. Mook, H. A., Sidis, Y., Fauqué, B., Balédent, V. & Bourges, P. Observation of magnetic order in a superconducting $YBa_2Cu_3O_{6.6}$ single crystal using polarized neutron scattering. *Phys. Rev. B* **78**, 020506 (2008).
13. Balédent, V. et al. Evidence for competing magnetic instabilities in underdoped $YBa_2Cu_3O_{6+x}$. *Phys. Rev. B* **83**, 104504 (2011).
14. Bourges, P. & Sidis, Y. Novel magnetic order in the pseudogap state of high-Tc copper oxides superconductors. *Comptes Rendus Phys.* **12**, 461–479 (2011).
15. Mangin-Thro, L., Li, Y., Sidis, Y. & Bourges, P. $a - b$ anisotropy of the intra-unit-cell magnetic order in $YBa_2Cu_3O_{6.6}$. *Phys. Rev. Lett.* **118**, 097003 (2017).
16. Jeong, J., Sidis, Y., Louat, A., Brouet, V. & Bourges, P. Time-reversal symmetry breaking hidden order in $Sr_2(Ir,Rh)O_4$. *Nat. Commun.* **8**, 15119 (2017).
17. Kaminski, A. et al. Spontaneous breaking of time-reversal symmetry in the pseudogap state of a high-Tc superconductor. *Nature* **416**, 610–613 (2002).
18. Zhang, J. et al. Discovery of slow magnetic fluctuations and critical slowing down in the pseudogap phase of $YBa_2Cu_3O_y$. *Sci. Adv.* **4**, eaao5235 (2018).
19. Varma, C. M. Theory of the pseudogap state of the cuprates. *Phys. Rev. B* **73**, 155113 (2006).

20. Agterberg, D. F., Melchert, D. S. & Kashyap, M. K. Emergent loop current order from pair density wave superconductivity. *Phys. Rev. B* **91**, 054502 (2015).
21. Chatterjee, S. & Sachdev, S. Insulators and metals with topological order and discrete symmetry breaking. *Phys. Rev. B* **95**, 205133 (2017).
22. Scheurer, M. S. & Sachdev, S. Orbital currents in insulating and doped antiferromagnets. *Phys. Rev. B* **98**, 235126 (2018).
23. Sarkar, S., Chakraborty, D. & Pépin, C. Incipient loop-current order in the underdoped cuprate superconductors. *Phys. Rev. B* **100**, 214519 (2019).
24. Lovesey, S. W., Khalyavin, D. D. & Staub, U. Ferro-type order of magneto-electric quadrupoles as an order-parameter for the pseudo-gap phase of a cuprate superconductor. *J. Phys.: Condens. Matter* **27**, 292201 (2015).
25. Lovesey, S. W. & Khalyavin, D. D. Ordered state of magnetic charge in the pseudo-gap phase of a cuprate superconductor ($HgBa_2CuO_{4+\delta}$). *J. Phys. Condens. Matter* **27**, 495601 (2015).
26. Fechner, M., Fierz, M. J., Thöle, F., Staub, U. & Spaldin, N. A. Quasistatic magnetoelectric multipoles as order parameter for pseudogap phase in cuprate superconductors. *Phys. Rev. B* **93**, 174419 (2016).
27. Varma, C. M. Pseudogap and Fermi arcs in underdoped cuprates. *Phys. Rev. B* **99**, 224516 (2019).
28. Chang, J. et al. Magnetic field controlled charge density wave coupling in underdoped $YBa_2Cu_3O_{6+x}$. *Nat. Commun.* **7**, 1–7 (2016).
29. Kim, H.-H. et al. Uniaxial pressure control of competing orders in a high-temperature superconductor. *Science* **362**, 1040–1044 (2018).
30. Badoux, S. et al. Change of carrier density at the pseudogap critical point of a cuprate superconductor. *Nature* **531**, 210–214 (2016).
31. Hsu, T. C., Marston, J. B. & Affleck, I. Two observable features of the staggered-flux phase at nonzero doping. *Phys. Rev. B* **43**, 2866–2877 (1991).
32. Chakravarty, S., Laughlin, R. B., Morr, D. K. & Nayak, C. Hidden order in the cuprates. *Phys. Rev. B* **63**, 094503 (2001).
33. Regnault, L., Bourges, P. & Burlet, P. in *Neutron Scattering in Layered Copper-Oxide Superconductors* (ed. Furrer, A.) 85–134 (Springer, 1998).
34. Stock, C. et al. Neutron scattering search for static magnetism in oxygen-ordered $YBa_2Cu_3O_{6.5}$. *Phys. Rev. B* **66**, 024505 (2002).
35. Andersen, N. et al. Superstructure formation and the structural phase diagram of $YBa_2Cu_3O_{6+x}$. *Phys. C: Superconductivity* **317**, 259–269 (1999).
36. Hinkov, V. et al. Two-dimensional geometry of spin excitations in the high-transition-temperature superconductor $YBa_2Cu_3O_{6+x}$. *Nature* **430**, 650–654 (2004).
37. Ito, T., Takenaka, K. & Uchida, S. Systematic deviation from T-linear behavior in the in-plane resistivity of $YBa_2Cu_3O_{7-y}$: Evidence for dominant spin scattering. *Phys. Rev. Lett.* **70**, 3995 (1993).
38. Suchaneck, A. et al. Incommensurate magnetic order and dynamics induced by spinless impurities in $YBa_2Cu_3O_{6.6}$. *Phys. Rev. Lett.* **105**, 037207 (2010).
39. Simon, M. E. & Varma, C. M. Detection and implications of a time-reversal breaking state in underdoped cuprates. *Phys. Rev. Lett.* **89**, 247003 (2002).
40. Shekhter, A. & Varma, C. M. Considerations on the symmetry of loop order in cuprates. *Phys. Rev. B* **80**, 214501 (2009).
41. Lim, S., Varma, C. M., Eisaki, H. & Kapitulnik, A. Observation of broken inversion and chiral symmetries in the pseudogap phase in single- and double-layer bismuth-based cuprates. *Phys. Rev. B* **105**, 155103 (2022).
42. Mesaros, A. et al. Topological defects coupling smectic modulations to intra-unit-cell nematicity in cuprates. *Science* **333**, 426–430 (2011).
43. Tang, Y. et al. Orientation of the intra-unit-cell magnetic moment in the high-T_c superconductor $HgBa_2CuO_{4+\delta}$. *Phys. Rev. B* **98**, 214418 (2018).
44. Wu, T. et al. Incipient charge order observed by NMR in the normal state of $YBa_2Cu_3O_y$. *Nat. Commun.* **6**, 6438 (2015).

Acknowledgements

We thank S. Davis, B. Fauqué, F. Krüger, A. Mesaros, C. Pépin and Y. Zaanen for stimulating discussions. We thank C.M Varma for bringing to us the illuminating perspectives of loop currents supercells. We acknowledge supports from the project NirvAna (contract ANR-14-OHRI-0010) of the French Agence Nationale de la Recherche (ANR) and from the GenLoop project of the LabEX PALM (contract ANR-10-LABX-0039-PALM). We also acknowledge financial support from the Fédération Française de Diffusion Neutronique (2FDN). The open access fee was covered by FILL2030, a European Union project within the European Commission's Horizon 2020 Research and Innovation program under grant agreement N°731096.

Author contributions

Y.S. and P.B. conceived and supervised the project; D.B., Y.S. and P.B. performed the experiments at LLB Saclay; D.B., V.B. and L.M.-T. performed the experiments at ILL Grenoble; F.B., M.B. and P.S. were the instrument local contacts and ILL. D.B. and P.B. analyzed the neutron data; T.L. prepared and characterized the detwinned single crystals sample; D.B., Y.S. and P.B. wrote the manuscript with further contributions from all authors. All authors contributed to this work, read the manuscript and agree to its contents.

Competing interests

The authors declare no competing interests.

Additional information

Supplementary information The online version contains supplementary material available at https://doi.org/10.1038/s42005-022-01048-1.

Correspondence and requests for materials should be addressed to Dalila Bounoua or Philippe Bourges.

Peer review information *Communications Physics* thanks the anonymous reviewers for their contribution to the peer review of this work. Peer reviewer reports are available.

Reprints and permission information is available at http://www.nature.com/reprints

Publisher's note Springer Nature remains neutral with regard to jurisdictional claims in published maps and institutional affiliations.